catalysts

MDPI

Article

Electrocatalytic Investigation by Improving the Charge Kinetics between Carbon Electrodes and Dopamine Using Bio-Synthesized CuO Nanoparticles

Shashanka Rajendrachari [1,*], Gururaj Kudur Jayaprakash [2,3], Anup Pandith [4,*], Abdullah Cahit Karaoglanli [1,5] and Orhan Uzun [6,7]

1 Department of Metallurgical and Materials Engineering, Bartin University, Bartin 74100, Turkey
2 Laboratory of Quantum Electrochemistry, School of Advanced Chemical Sciences, Shoolini University, Solan 173229, Himachal Pradesh, India
3 Department of Chemistry, Nitte Meenakshi Institute of Technology, Bangalore 560064, Karnataka, India
4 Department of International Ph.D. Program in Biomedical Engineering (IPBME), College of Biomedical Engineering, Taipei Medical University, Taipei City 11031, Taiwan
5 Turkish Airlines Inc., Istanbul 34149, Turkey
6 Bartin University, Bartin 74100, Turkey
7 Department of Physics, Ankara University, Ankara 06100, Turkey
* Correspondence: shashanka@bartin.edu.tr (S.R.); anuppandith@tmu.edu.tw (A.P.)

Abstract: We have successfully studied the charge transfer kinetics between carbon paste electrodes and dopamine using green synthesized rectangular monoclinic CuO nanoparticles (NPs) prepared by *Alchemilla vulgaris* leaves with the one-pot green synthesis method. The scanning electron microscopy (SEM) results confirmed the monoclinic structure with a particle size of around 85 nm. The investigation of thermal properties was carried out by thermogravimetric (TG) and differential thermal analysis (DTA). We also studied the electrochemical response of green synthesized CuO nanoparticles to detect Dopamine (DA) using cyclic voltammetry, which was proven to be an excellent electrocatalyst for the electro-oxidation of DA. The fabricated CuO nanoparticle modified carbon paste electrode (CMCPE) depicts fantastic selectivity, robustness, and sensitivity in analyzing DA in clinical and pharmaceutical preparations. The highest occupied molecular orbital (HOMO) and lowest unoccupied molecular orbital (LUMO) orbitals of the DA were studied using positive and negative charges at the CuO modified carbon paste electrode interface. Frontier molecular orbitals of DA are plotted to understand electron transfer reactivity at the electrode interface.

Keywords: CuO nanoparticles; charge kinetics; frontier molecular orbitals; cyclic voltammetry; dopamine sensor

Citation: Rajendrachari, S.; Kudur Jayaprakash, G.; Pandith, A.; Karaoglanli, A.C.; Uzun, O. Electrocatalytic Investigation by Improving the Charge Kinetics between Carbon Electrodes and Dopamine Using Bio-Synthesized CuO Nanoparticles. *Catalysts* **2022**, *12*, 994. https://doi.org/10.3390/catal12090994

Academic Editor: Nicolas Alonso-Vante

Received: 17 June 2022
Accepted: 29 August 2022
Published: 2 September 2022

1. Introduction

The biosynthesis of metal oxide nanoparticles is best known for its effective role in advancing the applications of nanomaterials in various domains. The study of nanomaterials requires a better apprehension of the crystal structure designed for specific applications and prepared from different synthesis methods [1]. In recent years, the exploration of metal oxide nanomaterials has become very popular because of their extensive properties and uses. The advantage of preparing metal oxide nanoparticles lies in their ability to produce extremely small (nanoscale), high surface area, unique physical and chemical properties. Nanoparticles of metal oxide may be prepared using different methods such as sol-gel, electrodeposition [2], ball milling [3–8], precipitation, combustion synthesis [9], and more. However, these approaches are cumbersome and costly and require additional environmentally and bio-dangerous specialized tools, high-temperature models, etc. During these methods, part of the harmful chemicals may adsorb on the nanoparticle surface and may

adversely affect medical applications; therefore, researchers are constantly working to synthesize nanoparticles with green methods [10].

This biosynthesis of metal oxide nanoparticles with regulated, customized structures is a simple, cost-effective, and environmentally sustainable process. The structure and properties of metal oxides depend primarily on solvent pH, solvent structure, experimental pressure, and temperature [11]. In recent years, various biological methods of synthesizing metal oxide nanoparticles have been developed [12]; however, using plant extract is proven to be a stable, faster, and extremely mono-dispersive method with high purity. Highly useful and diversified phytochemicals are the key reasons that a green synthesis approach has been selected [13].

CuO NPs, on the other hand, are an essential class of nanoparticles with specific features and innovative applications of metal oxide for electrochemical sensors [14], gas sensors, photodetectors, fungicides, antibacterial, antifouling, solar cells, water purifiers, coating, textiles, batteries, and catalysis [10]. Among metal oxide nanoparticles, CuO NPs have received significant attention from chemists, biologists, physicists, and metallurgists due to their high reactiveness, p-type semiconducting nature, high surface area, antibacterial properties, enzyme inhibition, and electrocatalytic properties; moreover, they are economical. Science experts have prepared CuO NPs using a variety of plants, but no one has reported the synthesis of CuO NPs using leaves of *Alchemilla vulgaris*. *Alchemilla vulgaris* is a common lady's mantle, whose Arabic name is Alkemelych, which means healing the many troubles [15]. The shape of the plant leaves resembles an animal foot, and therefore it is also famously called by names such as 'lion foot' and 'moon foot' [15]. It is also called Aslan Pençesi in Turkey, and it is served as an herbal tea and is useful for the digestive system, as well as being good for various ailments, such as sweating and restlessness, which may be experienced during the transition to menopause [15].

The biosynthesis of nanomaterials has huge advantages over other methods and can significantly impact the future of green synthesis of nanomaterials on an industrial scale where environmental contamination is an important concern [16]. Researchers are further trying to develop non-toxic, economical, and environmentally friendly processes by using a different variety of plants and preparing metal oxide nanoparticles. Throughout this article, the optical, thermal, and electrocatalytic properties of monoclinic CuO NPs have been effectively measured and tested. The green synthesized CuO NPs reported by various authors are tabulated in Table 1.

Table 1. Various researchers reported the synthesis of CuO nanoparticles using different plants.

Plant Name	Precursor	Average Size and Morphology	Featured Study	References
O. sanctum (Tulsi)	$Cu(CH_3COO)_2$	50 nm and flower shape	photocatalytic activity with H_2O_2 oxidant against degradation of methylene blue	[1]
Saraca indica	$CuCl_2{\cdot}H_2O$	40–70 nm and spherical	The photoluminescence behaviour	[10]
Adiantum lunulatum	$CuSO_4$	6–7 nm and quasi-spherical	Investigation of innate immunity, antioxidative enzymatic and oxidative stress of model plants such as Lens	[12]
Ocimum basilicum	$CuSO_4{\cdot}5H_2O$	70 nm and spherical	Antibacterial activity against *E. coli* and *S. aureus*	[16]
Tilia Tomentosa	$Cu(CH_3COO)_2$	113 nm and rod shape	Thermal and Antibacterial activity	[17]
Calotropis gigantean	$Cu(NO_3)_2$	20 nm and spherical	Dye-sensitized solar cells	[18]
Catharanthus Roseus	$CuSO_4$	5–10 nm and spherical	Studied the CuO membrane efficacy for chromium (VI) removal from waste water	[19]
Seidlitzia rosmarinus	$Cu(CH_3COO)_2$	222 nm and Cauliflower shape	Photocatalytic (degradation) and self-cleaning activity (decolouration) of methylene blue	[20]

Table 1. *Cont.*

Plant Name	Precursor	Average Size and Morphology	Featured Study	References
Gundelia tournefortii	$CuCl_2$	50–60 nm and spherical	The catalytic activity for the synthesis of N-monosubstituted urea and reduction of 4-nitrophenol	[21]
Gloriosa superba	$Cu(NO_3)_2$	5–10 nm and spherical	Antibacterial studies	[22]
Alchemilla vulgaris	$Cu(CH_3COO)_2$	85 nm and rectangular monoclinic	Thermal and electrochemical studies	Present paper

One important part of electrochemistry is the study of the electron transfer rate at the electrode–electrolyte interface. The reaction kinetics at the surface of the electrode plays an important role in understanding the heterogeneous electron transfer reactions [23]. We reported the electrode kinetics of CuO MCPE in dopamine which undergoes two-electron reactions. Dopamine (DA) is one of the crucial neurotransmitter molecules of catecholamines and its deficiency can cause brain disorders, such as schizophrenia and Parkinson's disease [3,4]. Therefore, detecting and analyzing the concentrations of dopamine and its metabolites is an essential goal in electrochemical analysis.

DA is an electrochemically active compound that is easily oxidizable; therefore, it can be determined by using electrochemical methods such as cyclic voltammetry (CV) [3,4]. Electrochemical researchers from the past few decades have given much more attention to designing and developing electrodes that exhibit significant molecular recognition capabilities. Many types of materials were used to design the electrode to detect neurotransmitter molecules. One of them is the CuO nanoparticle modified carbon paste electrode (CMCPE). Many researchers have used CuO NPs as a modifier, prepared from chemical or physical methods to detect bioactive compounds [14,24,25], but very limited literature is available on the use of nanoparticles prepared from plant extract as a modifier. After careful evaluation of these points, we can conclude that the proposed method is safe, robust, and eco-friendly. Hence, we proposed this green method as a novel approach for synthesizing CuO NPs and studying their optical, thermal, enzymatic inhibition, and electrocatalytic properties in detail. Our fabricated CMCPE showed excellent sensitivity and robustness towards the detection of dopamine even in the lowest concentrations.

2. Experimental

2.1. Preparation of Samples of Alchemilla vulgaris

Fresh leaves of *Alchemilla vulgaris* were purchased from Bartin, Turkey. The plant leaves were ground evenly using a blender. Then, 5 g of blended leaves were boiled for 15 min with 100 mL deionized water to obtain a clear, yellow-colored solution. To remove any impurities that had been stored, the yellow-colored solution was filtered and processed at 5 °C for future use. This extract is used for the preparation of rectangular monoclinic CuO NPs as seen in Figure 1.

2.2. Preparation of Rectangular Monoclinic CuO NPs

We prepared a homogeneous 2% copper acetate solution and added 5 mL of *Alchemilla vulgaris* extract dropwise with constant stirring at 80 °C for 10 min, which was accompanied by a steady shift of solution color from light blue to dark gray. This color change suggests the initial formation of CuO NPs. Then, 1M NaOH was added dropwise until the black color precipitate appeared upon stirring at 80 °C. The resultant solution was centrifuged at an rpm of 7500 at room temperature for 10 min. We then removed the supernatant solution followed by water wash and repeated the same procedure 3 to 4 times to remove any suspended impurities. Then, the centrifuged CuO NPs were placed overnight in an oven at 70 °C. To eliminate any evaporable impurities, the dried CuO NPs were further calcinated for 15 min at 400 °C.

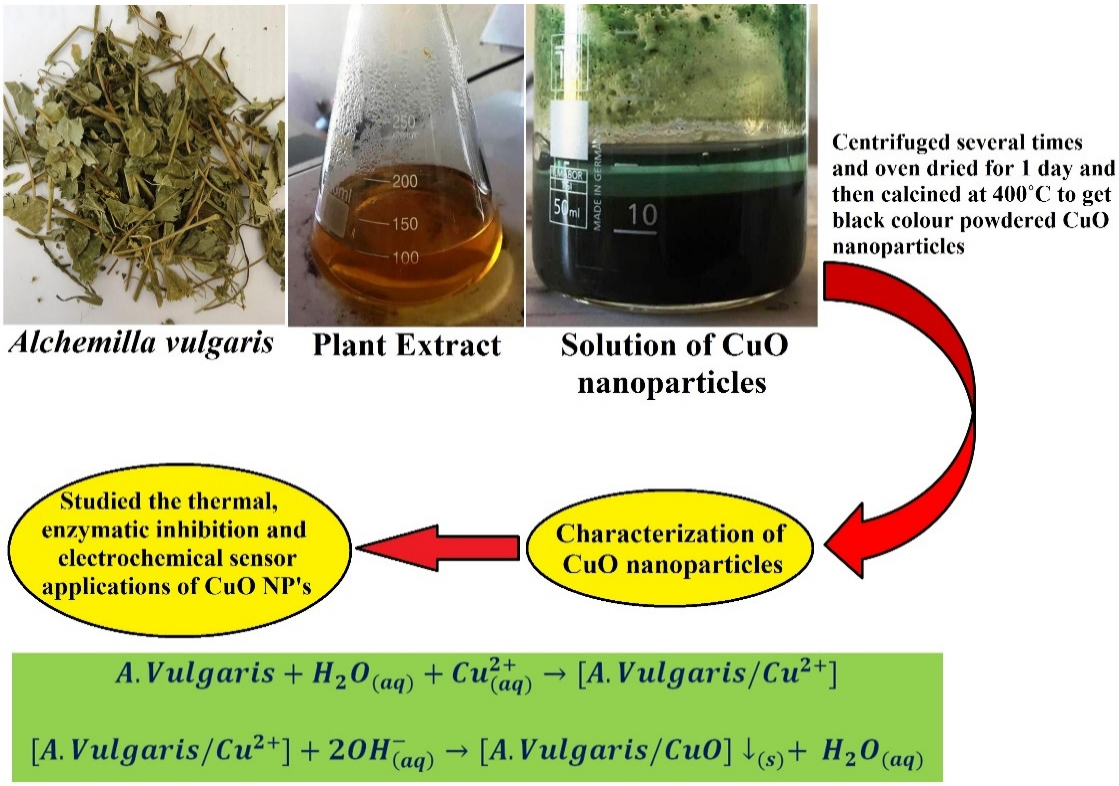

Figure 1. Experimental flowchart of green synthesis of CuO NPs using *Alchemilla vulgaris* leaves.

After the addition of NaOH to a Copper (II) acetate solution, the following chemical reaction took place to give CuO NPs [16].

$$\text{A. vulgaris} + H_2O_{(aq)} + Cu^{2+}_{(aq)} \rightarrow \left[\text{A. vulgaris}/Cu^{2+}\right] \quad (1)$$

$$\left[\text{A. vulgaris}/Cu^{2+}\right] + 2OH^-_{(aq)} \rightarrow [\text{A. vulgaris}/CuO] \downarrow_{(s)} + H_2O_{(aq)} \quad (2)$$

The precipitate of CuO was formed during the chemical reaction due to their high tendency of agglomeration to decrease the energy consorted with the huge surface area to volume ratio.

2.3. Fabrication of the Carbon Paste Electrode

The electro-catalytic analysis of CuO NPs was performed in the electrochemical workstation CHI-660c model provided with a conventional 3-electrode system comprised of a working electrode (CPE of 3 mm diameter), Ag/AgCl saturated KCl electrode as a reference electrode, and a platinum wire as counter electrode, respectively. The homogeneous bare carbon paste electrode (BCPE) was prepared by mixing the graphite powder and silicon oil at a ratio of 70:30 (*w/w*) in an agate mortar for 30 min. The fabricated paste was then closely tamped into a 3 mm cavity of a PVC tube attached to copper wire for the sake of electrical contact. CMCPE was prepared by spiking different concentrations of CuO NPs on the carbon paste. Figure 2 shows the pictorial representation of fabricating a green synthesized CMCPE.

2.4. Computational Methods

The DA structure was drawn using the Sinapsis [26] software tool as shown in Figure 3. Later, optimization of geometry was carried out using deMon2k [27,28] software with PBE [29,30] correlation functions and TZVP [31] basis sets. Finally, the plot of frontier molecular orbitals (FMO) was plotted using Sinapsis.

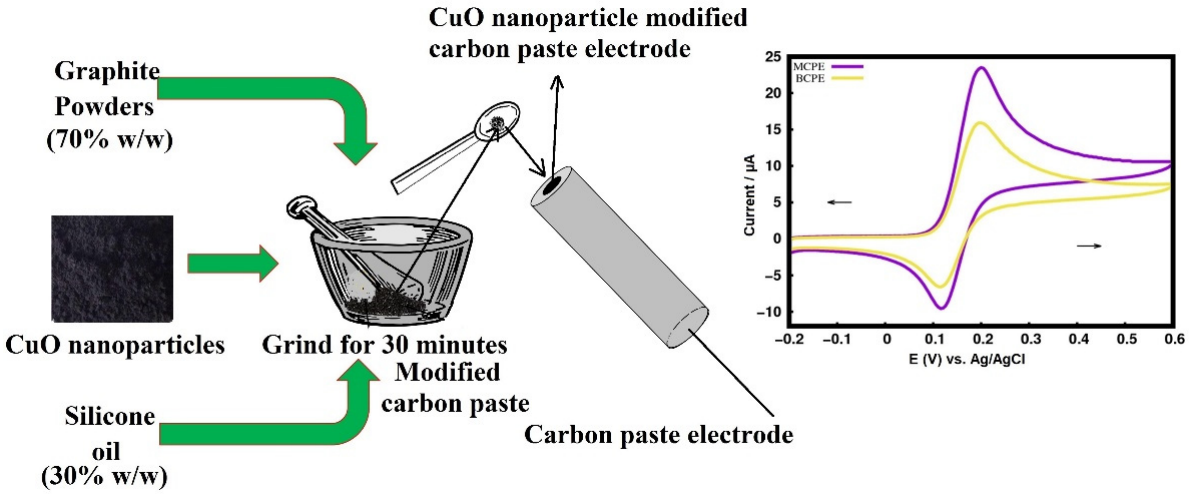

Figure 2. Graphical representation of fabricating green synthesized CuO nanoparticle modified carbon paste electrode.

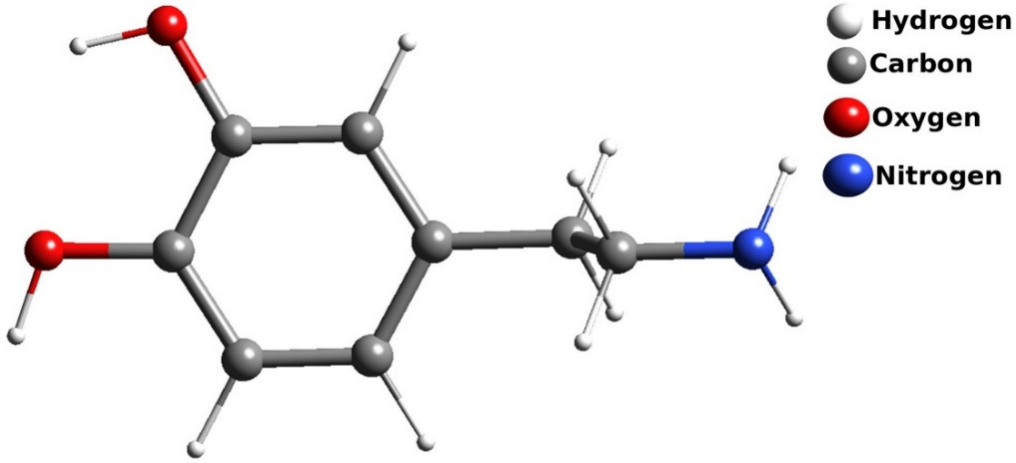

Figure 3. The DA structure drawn using Sinapsis software tool.

3. Results and Discussion

3.1. X-ray Diffraction (XRD)

The XRD diffraction of biosynthesized CuO NPs is depicted in Figure 4a. The diffraction peaks at 2θ of 35.54°, 38.85° corresponds to (002) and (111) planes with monoclinic structure as per the JCPDF Card No.: 01-080-1268. The XRD peaks depict the broad peaks due to the nanostructure of the prepared CuO NPs, more strain, and sometimes due to instrumental errors [32,33].

Scherrer formula was used to determine the average size of CuO crystallites [34]:

$$D = \frac{K\lambda}{\beta \cos \theta} \quad (3)$$

where

D = Average crystallite size,
K = 0.94, A constant
λ = Wavelength of X-ray (1.54 Å),
β = Full-width half maxima (in radians), and
2θ = Bragg angle (degrees).

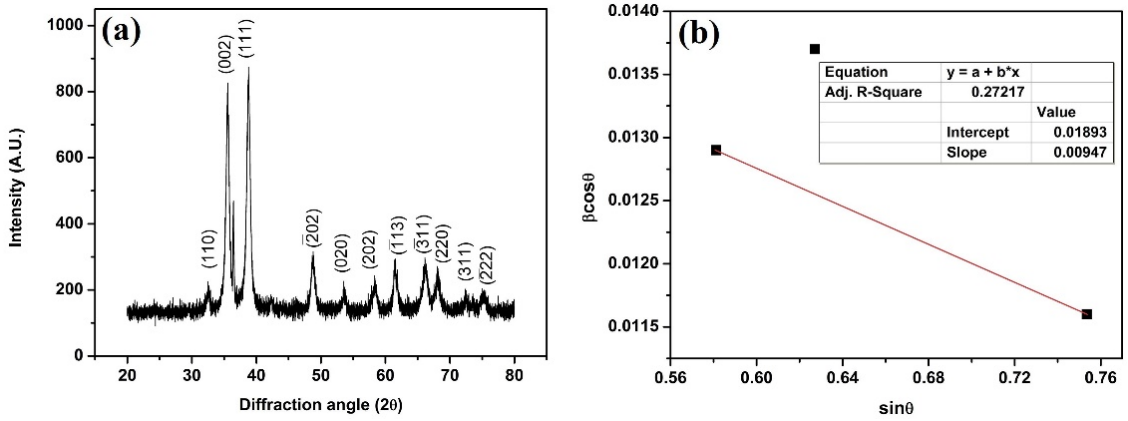

Figure 4. (**a**) XRD diffraction spectra of green synthesized CuO NPs, followed by (**b**) Williamson-Hall Plot to calculate lattice strain.

Using Scherrer's equation, we measured the crystallize scale for peaks (002) and (111) and found the average crystallite value to be equivalent to 10 nm. As per the report of Aparna et al., the particles that exhibit a crystallite size of less than 20 nm will show more lattice strain as compared with the particles having more than 20 nm crystallite size [35]. Therefore, we also calculated lattice strain using the Williamson–Hall (W-H) equation [36,37] as follows:

$$\beta \cos\theta = \frac{0.94\lambda}{D} + 4\varepsilon \sin\theta \quad (4)$$

β = Full width at half maximum (FWHM),
ε = Strain,
D = Crystallite size,
θ = Bragg's diffraction angle.

The sinθ and βcosθ values were plotted along the *x*-axis and *y*-axis, respectively. Figure 4b shows the W-H plot for CuO NPs prepared by *Alchemilla vulgaris* plant extract. The average sizes of crystallite and lattice strain were measured to be ~8 nm and 2.36×10^{-3}, respectively.

3.2. Scanning Electron Microscopy (SEM)

The SEM of biosynthesized monoclinic CuO NPs is shown in Figure 5a. The prepared CuO NPs show an almost rectangular shape with a monoclinic structure followed by a slight variation in their dimensions with an average particle size of 85 nm and no agglomerations. No reduction agents or extra capping agents are needed for this process since the *Alchemilla vulgaris* extract itself works as both and is, therefore, easy, economical, and environmentally friendly. Figure 5b shows the dark field scanning transmission electron microscopy (DF-STEM) image. Usually, DF-STEM is used to study the detailed morphology of the nanoparticles at higher magnification. Therefore, we have used STEM to reveal the structure and shape of the prepared CuO NPs. It was found that the result obtained from SEM is complemented with the results obtained from STEM. It also revealed no agglomeration of the CuO NPs with utmost homogeneity.

Figure 5c depicts the EDS picture of the nanoparticles formed in monoclinic CuO by the *Alchemilla vulgaris* extract. The EDS study was carried out to examine the qualitative and quantitative aspects of the CuO NPs. The figure confirms that copper and oxygen are both stoichiometric to each other experimentally and theoretically.

3.3. UV-Visible Spectroscopy

UV–visible spectroscopy typically utilizes light in both close to UV and near-infrared wavelengths, and molecules experience electrical changes in this visible range and influence

specifically the color change by the chemical components involved [38]. We used UV–visible light to analyze the optical properties in depth. The homogeneous solution of CuO NPs was prepared by dissolving them with de-ionized water by sonicating the solution for 2 min and exposing it to the light of a detectable spectrum. The resulting spectrum reveals a single strong absorption peak at 321 nm, which is seen in Figure 6.

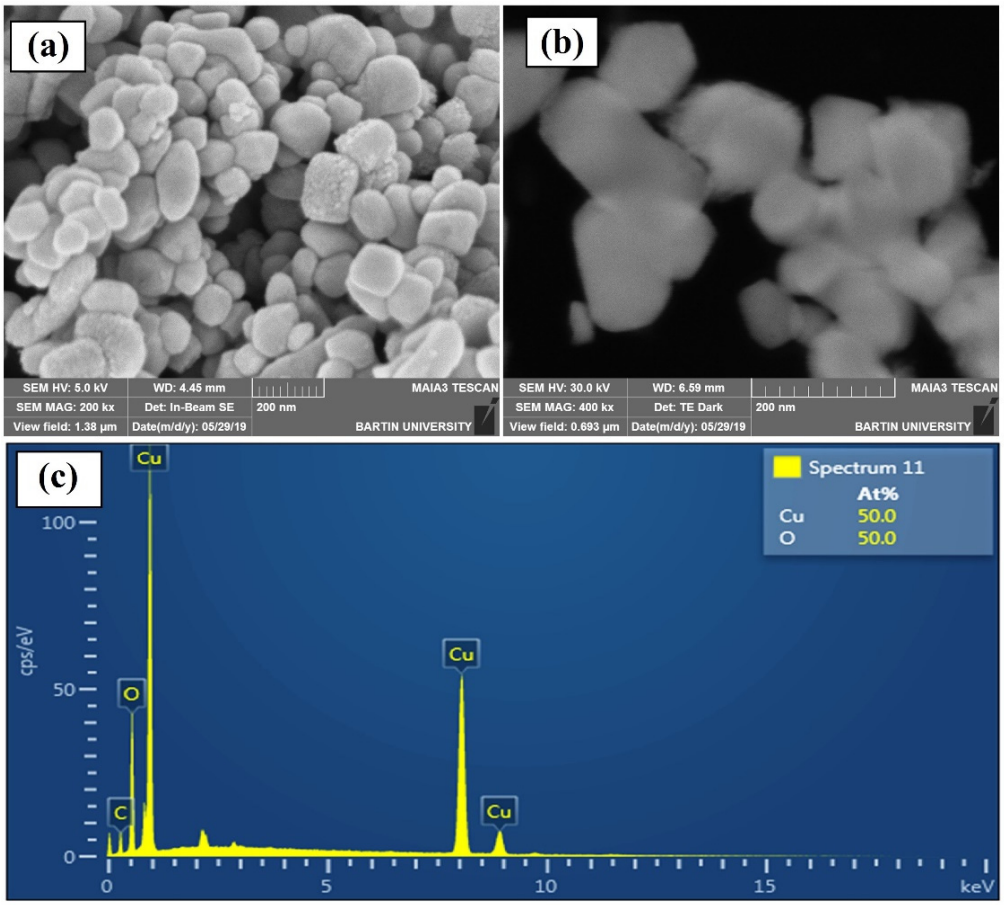

Figure 5. (**a**) SEM image of biosynthesized CuO NPs (**b**) Dark-field scanning transmission electron microscopy (DF-STEM) image (**c**) EDS image of CuO NPs.

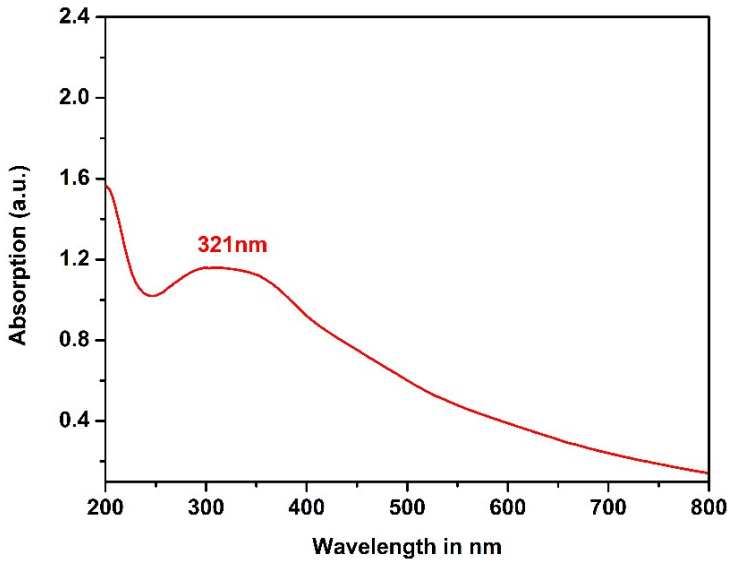

Figure 6. The UV-Visible spectra of green synthesized CuO NPs.

The maximum absorption degree is attributed to the absorption of CuO NPs and the reciprocal oscillation of the electrons of the free conduction band by electromagnetic radiation. Here, in this case, the wavelength of the incident light far exceeds the diameter of the CuO NPs; therefore, one can expect this type of resonance [39].

The energy bandgap (E) of the prepared CuO NPs was determined using the following equation [37,38]:

$$E = \frac{h \times C}{\lambda} \quad (5)$$

where

E = Bandgap energy

h = 6.626×10^{-34} Joules sec = Planks constant

C = 3.0×10^{8} m/sec = Speed of light

λ = 321×10^{-9} m = Cut off wavelength

* Conversion 1 eV = 1.6×10^{-19} Joules

The estimated energy value of the bandgap was 3.87 eV, higher than the CuO bandgap recorded [17,40]. This increase in bandgap energy is attributed to intra-gap conditions and the quantum containment effect [17].

3.4. Thermal Analysis

The thermal stability of bio-synthesized monoclinic copper oxide nanoparticles was analyzed at specific heating frequencies across a temperature spectrum of 30–1000 °C through TG and DTA. Figure 7a–c represents the TG and DTA plots of CuO NPs at a heating rate of 6, 8, and 10 °C/min, respectively. From the graphs, it is confirmed that the prepared CuO NPs show no phase transformation, high stability, and less weight loss. Owing to water evaporation and decomposition of organic content, just 2.1% weight loss was observed between 30 and 700 °C. The average weight reduction was calculated to be 11.5% during the heating cycle at 6 °C/min.

At 8 °C/min, just 1.9% weight loss was reported over 200–700 °C due to the water evaporation and the organic material decomposition. The average weight loss was estimated to be 11.3% at 8 °C/min. Likewise, a weight loss of 1.9% was reported at 200–800 °C, and a cumulative weight loss of 10.9% was observed for 10 °C/min heating rate. From the results, it was confirmed that the heating rate can affect the thermal stability of the prepared CuO NPs. As the heating rate increases, the weight reduction ratio falls from 11.5 to 10.9%. Therefore, we can conclude that the bio-synthesized CuO NPs exhibit extraordinary thermal stability over a wide temperature range (30–1000 °C) compared to other reported values [41,42].

We also studied the enthalpy change of CuO NPs using DTA. The DTA of the prepared CuO NPs was performed at a heating rate of 6, 8, and 10 °C/min, respectively, and these heating rates correspond to the respective endothermic peaks at 854, 871, and 877 °C as shown in Figure 7. All the endothermic peaks are due to the decomposition of organic matter and the conversion of CuO NPs to Cu_2O and Cu [17]. It has been found from the calculation that the decomposition peak shifts towards maximum temperatures at higher heating rates. This is due to the rise in enthalpy as well as the temperature at higher heating rates at the end of the cycle [17]. The change in enthalpy of the CuO NPs at 6, 8, and 10 °C/min was calculated and the values found to be 5.91, 2.54, and 1.22 kJ/mol, respectively. When the heating rate rises from 6 to 10 °C/min, the enthalpy also increases as seen in the figure.

The endothermic peaks of Figure 7 represent the decomposition, dehydration, and reduction of prepared CuO NPs at higher temperatures. Table 2 depicts the calculated weight reduction, decomposition peak temperature, and enthalpy shift in prepared CuO NPs.

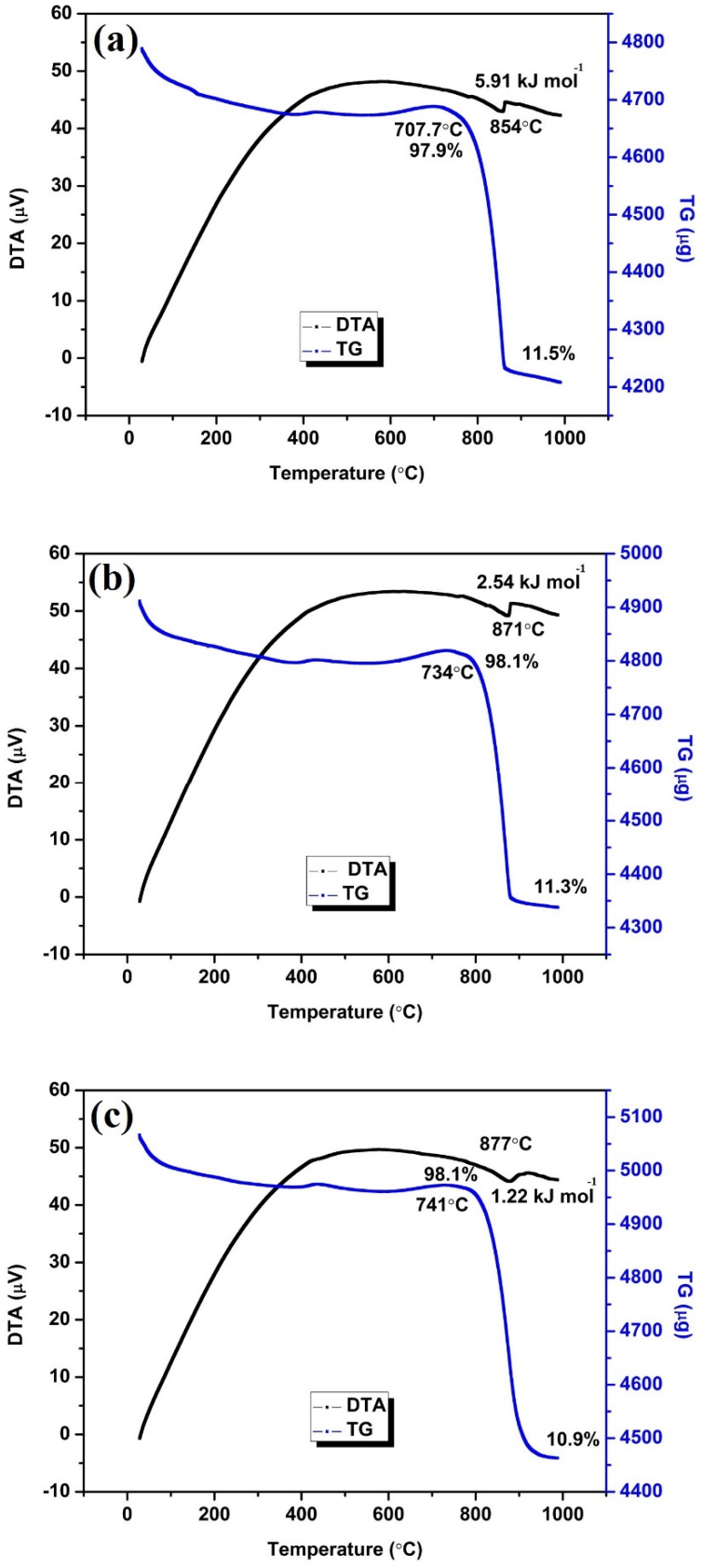

Figure 7. Thermogravimetric and differential thermal analysis curve of biosynthesized CuO NPs at (**a**) 6 °C/min (**b**) 8 °C/min and (**c**) 10 °C/min heating rates respectively.

Table 2. The total weight loss, decomposition peak temperature, and enthalpy change of the CuO nanoparticles calculated using TG and DTA curves.

Type of Nanomaterial	Heating Rate (°C/min)	Decomposition Temperature (°C)	Percentage Weight Loss	* Enthalpy Change (kJ/mol)
CuO nanoparticles	6	854	11.5	5.91
	8	871	11.3	2.54
	10	877	10.9	1.22

* Converted values of mJ/mg to kJ/mol.

3.5. Electrocatalytic Property of Dopamine (DA) at MCPE

3.5.1. Electrocatalytic Property of CuO for Determining Dopamine (DA)

One of the very important steps in designing a modified carbon paste electrode is selecting a proper concentration of redox catalysts showing the highest sensitivity. Nanoparticles can improve the performance of CPE. In particular, some studies have been conducted on improving the sensing abilities of CPE from CuO NPs [14,24]. However, previously proposed electrodes were constructed using chemically derived CuO NPs. In the present work, we have used eco-friendly, biosynthesized CuO NPs.

Figure 8a shows a graph of various concentrations of CuO NPs along with their respective anodic peak currents. The plot confirms that the anodic peak current Ipa (A) increases with the CuO NPs (modifier) concentration up to 6 mg and then it decreases with further increase in the concentration, and this is due to the decreased number of oxidation sites and the actual electrode area [43]. Therefore, the CuO nanoparticle modifier was used to enhance the anodic peak current and to decrease the overpotential.

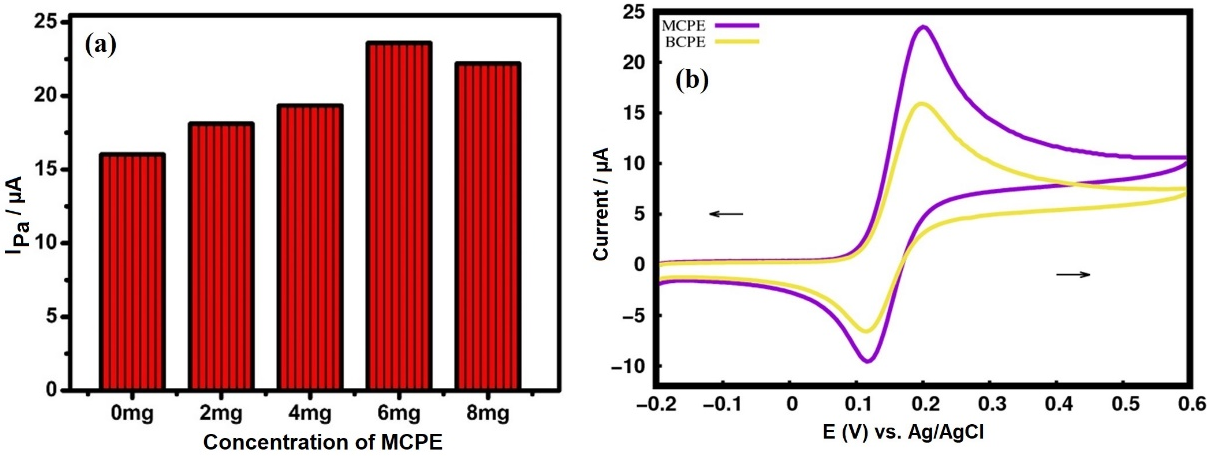

Figure 8. (**a**) A graph of various concentrations of CuO NPs along with their respective anodic peak currents. (**b**) The cyclic voltammogram of BCPE and 6 mg concentration of the CMCPE at 2 mM DA concentration.

The cyclic voltammogram of 0.1 mM DA at BCPE and CuO-MCPE is shown in Figure 8b. The Ipa of BCPE was lower than the CuO-MCPE, and the ΔEp values are lower at the CuO-MCPE. We have also compared the ΔEp of different CuO nanoparticle-modified electrodes from different reports. However, our method shows lower ΔEp. Therefore, biosynthesized CuO NPs are comparatively better than chemically synthesized nanoparticles. As a part of the work, the active surface area of the CuO-MCPE was calculated using Equation (5) [27].

$$i_p = 2.69 \times 10^5\, n^{3/2} A D^{1/2} C \nu^{1/2} \quad (6)$$

where i_p is the peak current, A is the electroactive area (cm^2), C is the concentration of the electroactive species (mol cm^{-3}), n is the number of exchanged electrons (2), D is the

diffusion coefficient ($cm^2\ s^{-1}$), and υ is the scan rate ($V\ s^{-1}$). The active surface area for the ET process of DA is 0.042 cm^2 and 0.077 cm^2 for the bare and MCPE, respectively.

At the CuO-MCPE interface, Cu lattices of CuO crystals have a positive charge, which will attract electron-rich sites of dopamine (possibly from HOMO of DA). Similarly, negative charges at the CuO electrode interface can donate electrons to electron-deficient sites of dopamine (possibly LUMO of DA). Therefore, we have plotted the frontier molecular orbitals of DA. Frontier molecular orbitals of DA are shown in Figure 9. The HOMO and LUMO orbitals of the DA are shown in Figures 9a and 9b, respectively. Thus, our studies help to understand the electron transfer process between DA and CuO modified electrodes.

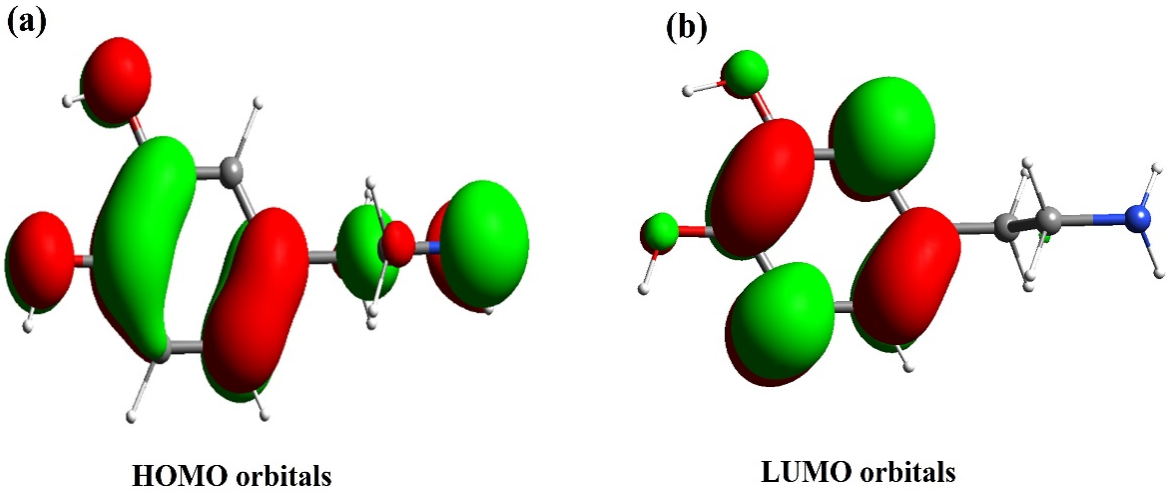

Figure 9. Frontier molecular orbitals.

3.5.2. Effect of Scan Rate

The scan rate was used to investigate the effect on the intensity of the peak current by knowing whether the redox process is diffusion or adsorption controlled. We studied the kinetics of the electrode reaction at different scan rates of 100, 150, 250, 350, and 400 mVs^{-1}. Figure 10a depicts cyclic voltammograms recorded for DA at different scan rates at 6 mg MCPE in a phosphate buffer solution (PBS) of pH 7.2. The cyclic voltammogram confirms the linear increase of Ipa with an increasing scan rate. This increasing trend is due to the direct electron transfer between the analyte (DA) and the surface of MCPE. Figure 10b,c shows the plot of the Ipa vs. scan rate and Ipa vs. square root of scan rate; their correlation coefficient was determined to be 0.9976 and 0.9975, respectively. Therefore, the mass transfer process is both adsorption and diffusion-controlled [27].

Using Marcus's free energy-rate relation, Tender et al. [44] and Ingram et al. [45] explicated the electrode kinetics theory of surface-immobilized monolayers using CV. Within the boundary of this theory, it is possible to calculate the standard rate constant (k^0) using experimental ΔEp values [46]. This calculation complies with a Marcus-DOS model which integrates the Marcus equation over electronic states as shown below [46]:

$$K_\eta = \mu\rho K_B T \int_{-\infty}^{\infty} \frac{\exp\left[-\left(x - \frac{\lambda \pm \eta}{K_B T}\right)^2 \left(\frac{K_B T}{4\lambda}\right)\right]}{1 + \exp(x)} dx \quad (7)$$

where

K_η = The rate constant at the electrode over-potential η
λ = The reorganization barrier energy
μ = pre-exponential factor including the distance-dependent electronic coupling parameter
ρ = The density of electronic states in the metal electrode.

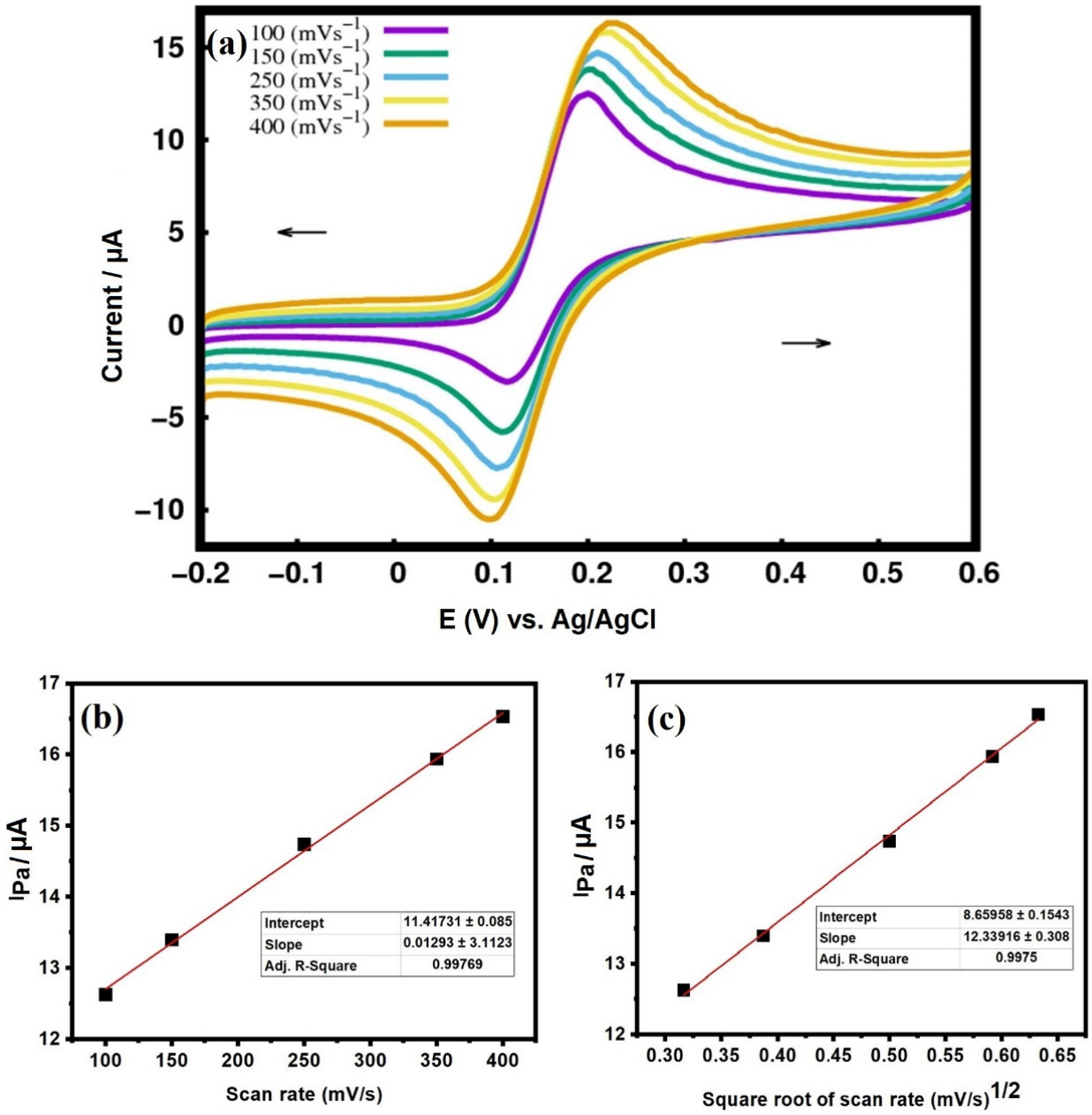

Figure 10. (**a**) The cyclic voltammogram at 6 mg CMCPE at 2 mM dopamine concentration in a phosphate buffer solution (PBS) of pH 7.2. (**b**) Plot of anodic peak current vs. scan rate (**c**) Plot of anodic peak current vs. square root of scan rate.

Using Equation (5), Tender et al. [44] digitally simulated cyclic voltammograms to explicate working curves of ΔEp vs. log (υ/k^0) based on some assumption values of λ. One such working curve is Equation (5), which is used to calculate the values of k^0 from experimental ΔEp values; and this equation is well operated when ΔEp > 10 mV. Therefore, we calculated the heterogeneous rate constant (k^0) values for DA using ΔEp and υ from the experimental data. The calculated k^0 values for DA at the different scan rates of 100 to 400 mV/s were tabulated in Table 3.

$$\Delta Ep = 201.39 \log\left(\frac{\vartheta}{k^0}\right) - 301.78 \quad (8)$$

where

ΔEp = Potential difference between the cathodic and anodic peak potentials

υ = Potential scan rate
k^0 = Standard electron-transfer rate at the zero over-potential

Table 3. The calculated k^0 values for DA at the different experimental scan rates and ΔEp respectively using CuO MCPE and BCPE.

Type of Electrode	Scan Rate (mV/s)	ΔEp	k^0 (S^{-1})
CuO MCPE	100	79	1.28
CuO MCPE	150	87	1.76
CuO MCPE	250	103	2.44
CuO MCPE	350	114	3.02
CuO MCPE	400	129	2.88
BCPE	50	86	0.59

As per the calculated k^0 values, CuO MCPE shows a higher maximum rate constant than BCPE. The k^0 is more at 350 mV/s scan rate compared to other scan rates. The rate constant values obtained using CuO-MCPE are more than the reported values using different modifiers as shown in Table 4.

Table 4. The maximum rate constant K^0 values reported by various researchers for DA using different modifiers.

Modifier Used	Scan Rate (υ) at Which the Maximum k^0 is Recorded (mV/s)	Rate Constant, k^0 (s^{-1})	References
TiO_2 Nanorods	100	1.17	[47]
CuO nanoparticles	100	1.023	[24]
Graphene oxide	100	0.99	[48]
Gold nanoparticles	100	4.25×10^{-2}	[49]
Tungsten oxide nanoparticles	100	0.604	[50]
CuO nanoparticles	100	1.28	[Present paper]

3.5.3. Effect of pH Variation

The proper selection of pH improves the performance of an electrode [51,52]. Figure 11a shows the cyclic voltammograms collected from the 6 mg CuO-MCPE in 0.1 mM DA and 0.2 M PBS with a scan rate of 100 mVs^{-1} at different pH. Voltammogram confirms the increased anodic peak potential of DA with pH. The pH 7.2 was considered as the optimum pH value and performed all the electrochemical studies at this pH. Figure 11b represents the plot of pH vs. Ipa potential at 2 mM DA. From the plot, it is confirmed that the anodic peak potential increases gradually from pH 5.7 to 8 with a correlation coefficient of 0.9918. The graph obeys the Nernst equation with its slope equal to 61.8 mV/pH and therefore, we can conclude that an equal number of electrons and protons are involved in the transfer reaction.

3.5.4. Effect of Variation in DA Concentration

The effect of the DA concentration was studied using MCPE. With an increase in the concentration of DA, Ipa also increased linearly. In the present study, we have reported the electrochemical response of DA from 0.1 to 0.4 mM DA. Figure 12a shows the cyclic voltammogram of various concentrations of DA in a PBS of pH 7.2 at the MCPE. The DA concentration and Ipa are directly proportional to each other, and both increase linearly as shown in Figure 12b. This linear increase of Ipa is due to the sequential increase in the number of DA molecules at the MCPE interface [53].

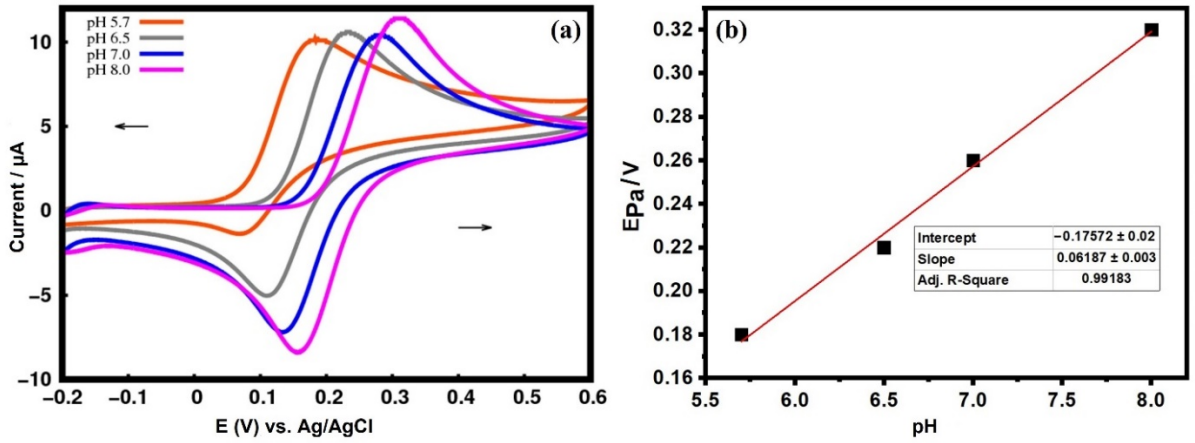

Figure 11. (**a**) The cyclic voltammogram of different pH (**b**) Plot of anodic peak potential vs. different pH.

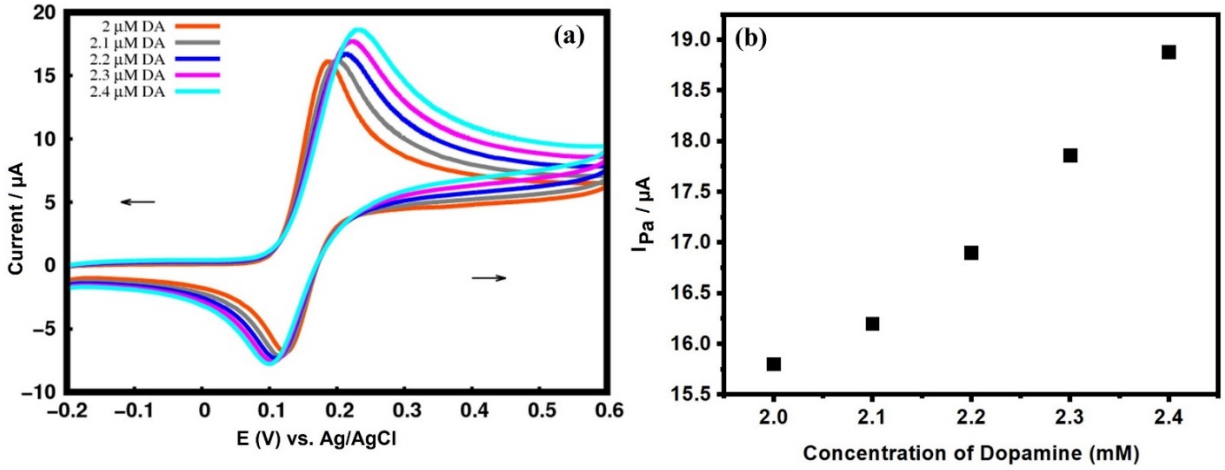

Figure 12. (**a**) The cyclic voltammogram of different concentration of DA. (**b**) Plot of anodic peak current vs. different concentration of DA.

4. Conclusions

The monoclinic CuO NPs were prepared by a plant-mediated method using extracts of *Alchemilla vulgaris* leaves. The XRD spectrum confirms the average crystallite size of ~8 nm and the lattice strain of 2.36×10^{-3}, respectively. The UV–visible spectrum depicts a single broad absorption peak at 321 nm followed by bandgap calculations, and the value was found to be 3.87 eV. The thermogravimetric analysis shows that the biosynthesized CuO NPs are highly stable and involve less material loss. The DTA curves show the endothermic peaks at 854, 871, and 877 °C at 6, 8, and 10 °C/min heating rates, respectively. The variability in enthalpy of biosynthesized CuO NPs was observed to be 5.91, 2.54, and 1.22 kJ/mol, respectively at the above heating rates. The green synthesized CuO NPs were used to improve the performance of the carbon paste electrode. The green CuO nanoparticle modifier increased the anodic peak current by decreasing the overpotential. However, our green synthesized CuO NPs showed lower ΔEp and compared to chemically synthesized nanoparticles. In a CuO modified carbon paste electrode interface, the Cu lattices of CuO crystals show a positive charge and attract electron-rich sites of dopamine (possibly HOMO of DA). Similarly, negative charges at the CuO electrode interface attract less electron-rich sites of dopamine (possibly LUMO of DA). The k^0 value obtained using CuO MCPE is more than the reported values. and this improves the electron transfer between carbon paste electrodes and dopamine. Therefore, the fabricated CuO MCPE is proven to be an excellent, low-cost, and green electrocatalyst used to detect DA.

Author Contributions: Conceptualization, methodology, writing—original draft preparation, supervision, S.R.; software, validation, G.K.J.; formal analysis, supervision, A.P.; resources, project administration, data curation, A.C.K.; funding acquisition, resources, O.U. All authors have read and agreed to the published version of the manuscript.

Funding: The authors gratefully acknowledge Bartin University Scientific Research Projects Unit, Turkey for providing financial support to conduct the research (Project number: 2019-FEN-A-006).

Data Availability Statement: Not applicable.

Acknowledgments: Anup Pandith, thankful to International Ph.D. Program in Biomedical Engineering (IPBME), Taipei Medical University for providing financial assistance through the newly hired faculty Research project No.: TMU111-AE1-B10.

Conflicts of Interest: The authors declare no conflict of interest.

References

1. Siddiqui, H.; Qureshi, M.S.; Haque, F.Z. Biosynthesis of Flower-Shaped CuO Nanostructures and Their Photocatalytic and Antibacterial Activities. *Nano-Micro Lett.* **2020**, *12*, 29. [CrossRef]
2. Reddy, S.; Swamy, B.E.K.; Aruna, S.; Kumar, M.; Shashanka, R.; Jayadevappa, H. Preparation of NiO/ZnO hybrid nanoparticles for electrochemical sensing of dopamine and uric acid. *Chem. Sens.* **2012**, *2*, 1–7.
3. Shashanka, R.; Chaira, D.; Swamy, B.E.K. Fabrication of yttria dispersed duplex stainless steel electrode to determine dopamine, ascorbic and uric acid electrochemically by using cyclic voltammetry. *Int. J. Sci. Eng. Res.* **2016**, *7*, 1275–1285.
4. Shashanka, R.; Chaira, D.; Swamy, B.E.K. Electrochemical investigation of duplex stainless steel at carbon paste electrode and its application to the detection of dopamine, ascorbic and uric acid. *Int. J. Sci. Eng. Res.* **2015**, *6*, 1863–1871.
5. Shashanka, R.; Chaira, D.; Swamy, B.E.K. Electrocatalytic Response of Duplex and Yittria Dispersed Duplex Stainless Steel Modified Carbon Paste Electrode in Detecting Folic Acid Using Cyclic Voltammetry. *Int. J. Electrochem. Sci.* **2015**, *10*, 5586–5598.
6. Gupta, S.; Rajendrachari, S.; Chaira, D. Synthesis of nano-structured duplex and ferritic stainless steel powders by planetary milling: An experimental and simulation study. *IOP Conf. Ser. Mater. Sci. Eng.* **2015**, *75*, 012033. [CrossRef]
7. Nayak, A.K.; Rajendrachari, S.; Chaira, D. Effect of Nanosize Yittria and Tungsten Addition to Duplex Stainless Steel During High Energy Planetary Milling. *IOP Conf. Ser. Mater. Sci. Eng.* **2016**, *115*, 012008. [CrossRef]
8. Rajendrachari, S. Synthesis of nano-structured stainless steel powder by mechanical alloying-an overview. *Int. J. Sci. Eng. Res.* **2017**, *8*, 588–594.
9. Shashanka, R.; Kamaci, Y.; Tas, R.; Ceylan, Y.; Bülbül, A.S.; Uzun, O.; Karaoglanli, A.C. Antimicrobial investigation of CuO and ZnO nanoparticles prepared by a rapid combustion method. *Phys. Chem. Res.* **2019**, *7*, 799–812.
10. Prasad, K.S.; Patra, A.; Shruthi, G.; Chandan, S. Aqueous Extract of Saraca indica Leaves in the Synthesis of Copper Oxide Nanoparticles: Finding a Way towards Going Green. *J. Nanotechnol.* **2017**, *2017*, 7502610. [CrossRef]
11. Singh, J.; Dutta, T.; Kim, K.H.; Rawat, M.; Samddar, P.; Kumar, P. Green synthesis of metals and their oxide nanoparticles: Applications for environmental remediation. *J. Nanobiotechnol.* **2018**, *16*, 84. [CrossRef] [PubMed]
12. Sarkar, J.; Chakraborty, N.; Chatterjee, A.; Bhattacharjee, A.; Dasgupta, D.; Acharya, K. Green Synthesized Copper Oxide Nanoparticles Ameliorate Defence and Antioxidant Enzymes in Lens culinaris. *Nanomaterials* **2020**, *10*, 312. [CrossRef] [PubMed]
13. Doble, M.; Kruthiventi, A.K. *Green Chemistry and Engineering*; Elsevier Inc.: Amsterdam, The Netherlands, 2007.
14. Rajendrachari, S.; Swamy, B.E.K. Simultaneous electro-generation and electrodeposition of copper oxide nanoparticles on glassy carbon electrode and its sensor application. *SN Appl. Sci.* **2020**, *2*, 956.
15. Tobyn, G.; Denham, A.; Whitelegg, M. Alchemilla vulgaris, lady's mantle. In *Medicinal Herbs*; Elsevier: Amsterdam, The Netherlands, 2011; pp. 57–65.
16. Gültekin, D.D.; Güngör, A.A.; Önem, H.; Babagil, A.; Nadaroğlu, H. Synthesis of Copper Nanoparticles Using a Different Method: Determination of Its Antioxidant and Antimicrobial Activity. *J. Turk. Chem. Soc. Sect. A Chem.* **2016**, *3*, 623. [CrossRef]
17. Shashanka, R.; Yilmaz, V.M.; Karaoglanli, A.C.; Uzun, O. Investigation of activation energy and antibacterial activity of CuO nano-rods prepared by Tilia Tomentosa (Ihlamur) leaves. *Moroc. J. Chem.* **2020**, *8*, 497–509.
18. Sharma, J.K.; Akhtar, M.S.; Ameen, S.; Srivastava, P.; Singh, G. Green synthesis of CuO nanoparticles with leaf extract of Calotropis gigantea and its dye-sensitized solar cells applications. *J. Alloys Compd.* **2015**, *632*, 321–325. [CrossRef]
19. Choudhury, P.; Mondal, P.; Majumdar, S.; Saha, S.; Sahoo, G.C. Preparation of ceramic ultrafiltration membrane using green synthesized CuO nanoparticles for chromium (VI) removal and optimization by response surface methodology. *J. Clean. Prod.* **2018**, *203*, 511–520. [CrossRef]
20. Rezaie, A.B.; Montazer, M.; Rad, M.M. Photo and biocatalytic activities along with UV protection properties on polyester fabric through green in-situ synthesis of cauliflower like CuO nanoparticles. *J. Photochem. Photobiol. B Biol.* **2017**, *176*, 100–111. [CrossRef]
21. Nasrollahzadeh, M.; Maham, M.; Sajadi, S.M. Green synthesis of CuO nanoparticles by aqueous extract of Gundelia tournefortii and evaluation of their catalytic activity for the synthesis of N-monosubstituted ureas and reduction of 4-nitrophenol. *J. Colloid Interface Sci.* **2015**, *455*, 245–253. [CrossRef]

22. Naika, H.R.; Lingaraju, K.; Manjunath, K.; Kumar, D.; Nagaraju, G.; Suresh, D.; Nagabhushana, H. Green synthesis of CuO nanoparticles using Gloriosa superba L. extract and their antibacterial activity. *J. Taibah Univ. Sci.* **2015**, *9*, 7–12. [CrossRef]
23. Bhatti, N.K.; Subhani, M.S.; Khan, A.Y.; Qureshi, R.; Rahman, A. Heterogeneous Electron Transfer Rate Constants of Viologen Monocations at a Platinum Disk Electrode. *Turk. J. Chem.* **2006**, *30*, 165–180.
24. Reddy, S.; Swamy, B.E.K.; Jayadevappa, H. CuO nanoparticle sensor for the electrochemical determination of dopamine. *Electrochim. Acta* **2012**, *61*, 78–86. [CrossRef]
25. Ghodsi, J.; Rafati, A.A.; Shoja, Y.; Najafi, M. Determination of Dopamine in the Presence of Uric Acid and Folic Acid by Carbon Paste Electrode Modified with CuO Nanoparticles/Hemoglobin and Multi-Walled Carbon Nanotube. *J. Electrochem. Soc.* **2015**, *162*, B69–B74. [CrossRef]
26. Flores-Moreno, R.; Urbina, K.P.; Sandoval, Z.G. *Sinapsis, Version XII-V*; Sinapsis Developers: Guadalajara, Mexico, 2012.
27. Koster, A.M.; Geudtner, G.; Calaminici, P.; Casida, M.E.; Dominguez, V.D.; Flores-Moreno, R.; Gamboa, G.U.; Goursot, A.; Heine, T.; Ipatov, A.; et al. *deMon Developers, deMon2k*; Version 3; Cinvestav: Mexico City, Mexico, 2011.
28. Gerald, G.; Patrizia, C.; Javier, C.; del Campo, J.M.D.D.V.; Flores, M.R.; Ulises, G.G.; Annick, G.; Koster, A.M.; Ulises, R.J.; Tzonka, M.; et al. demon2k. *Wiley Interdiscip. Rev. Comput. Mol. Sci.* **2012**, *2*, 548–555.
29. Perdew, J.P.; Burke, K.; Ernzerhof, M. Generalized Gradient Approximation Made Simple. *Phys. Rev. Lett.* **1997**, *78*, 1396. [CrossRef]
30. Salahub, D.R.; Noskov, S.Y.; Lev, B.; Zhang, R.; Ngo, V.; Goursot, A.; Calaminici, P.; Köster, A.M.; Alvarez-Ibarra, A.; Mejía-Rodríguez, D.; et al. QM/MM Calculations with deMon2k. *Molecules* **2015**, *20*, 4780–4812. [CrossRef] [PubMed]
31. Godbout, N.; Salahub, D.R.; Andzelm, J.; Wimmer, E. Optimization of Gaussian-type basis sets for local spin density functional calculations. Part I. Boron through neon, optimization technique and validation. *Can. J. Chem.* **1992**, *70*, 560–571. [CrossRef]
32. Rajendrachari, S.; Swamy, B.E.K.; Reddy, S.; Chaira, D. Synthesis of Silver Nanoparticles and their Applications. *Anal. Bioanal. Electrochem.* **2013**, *5*, 455–466.
33. Rajendrachari, S. Investigation of Electrochemical Pitting Corrosion by Linear Sweep Voltammetry: A Fast and Robust Approach. In *Voltammetry*; IntechOpen: London, UK, 2019; pp. 77–90.
34. Shashanka, R.; Esgin, H.; Yilmaz, V.M.; Caglar, Y. Fabrication and characterization of green synthesized ZnO nanoparticle based dye-sensitized solar cells. *J. Sci. Adv. Mater. Devices* **2020**, *5*, 185–191. [CrossRef]
35. Aparna, Y.; Rao, K.V.E.; Subbarao, P.S. Synthesis and Characterization of CuO Nano Particles by Novel Sol-Gel Method. *J. Nano-Electron. Phys.* **2012**, *4*, 03005.
36. Shashanka, R. Effect of Sintering Temperature on the Pitting Corrosion of Ball Milled Duplex Stainless Steel by using Linear Sweep Voltammetry. *Anal. Bioanal. Electrochem.* **2018**, *10*, 349–361.
37. Rajendrachari, S.; Karaoglanli, A.C.; Ceylan, Y.; Uzun, O. A fast and robust approach for the green synthesis of spherical Magnetite (Fe_3O_4) nanoparticles by Tilia Tomentosa (Ihlamur) leaves and its antibacterial studies. *Pharm. Sci.* **2020**, *26*, 175–183. [CrossRef]
38. Shashanka, R.; Ceylan, K.B. The activation energy and antibacterial investigation of spherical Fe_3O_4 nanoparticles prepared by Crocus sativus (Saffron) flowers. *Biointerface Res. Appl. Chem.* **2020**, *10*, 5951–5959.
39. Das, D.; Nath, B.C.; Phukon, P.; Dolui, S.K. Synthesis and evaluation of antioxidant and antibacterial behavior of CuO nanoparticles. *Colloids Surf. B Biointerfaces* **2013**, *101*, 430–433. [CrossRef] [PubMed]
40. Dodoo-Arhin, D.; Leoni, M.; Scardi, P. Microemulsion Synthesis of Copper Oxide Nanorod-Like Structures. *Mol. Cryst. Liq. Cryst.* **2012**, *555*, 17–31. [CrossRef]
41. Manjari, G.; Saran, S.; Arun, T.; Rao, A.V.B.; Devipriya, S.P. Catalytic and recyclability properties of phytogenic copper oxide nanoparticles derived from Aglaia elaeagnoidea flower extract. *J. Saudi Chem. Soc.* **2017**, *21*, 610–618. [CrossRef]
42. Kayani, Z.N.; Umer, M.; Riaz, S.; Naseem, S. Characterization of Copper Oxide Nanoparticles Fabricated by the Sol–Gel Method. *J. Electron. Mater.* **2015**, *44*, 3704–3709. [CrossRef]
43. Gururaj, K.J.; Swamy, B.E.K.; Casillas, N.; Flores-Moreno, R. Analytical Fukui and cyclic voltammetric studies on ferrocene modified carbon electrodes and effect of Triton X-100 by immobilization method. *Electrochim. Acta* **2017**, *258*, 1025–1034.
44. Tender, L.; Carter, M.T.; Murray, R.W. Cyclic Voltammetric Analysis of Ferrocene Alkanethiol Monolayer Electrode Kinetics Based on Marcus Theory. *Anal. Chem.* **1994**, *66*, 3173–3181. [CrossRef]
45. Ingram, R.S.; Murray, R.W. Electron Transfer Kinetics of Ferrocene Alkanethiolate Monolayers in Ether and Poly-ether Solvents. *Faraday Trans. Roy. Soc. Chem.* **1996**, *92*, 3946.
46. Silvia, C.-A.; Georgina, A.-A.; Maria Teresa, R.-S.; Giselle, R.-P.; Mario, R.-R.; Manuel, P.-P. On the electrochemistry of dopamine in aqueous solution. Part I: The role of [SDS] on the voltammetric behavior of dopamine on a carbon paste electrode. *J. Electroanal. Chem.* **2007**, *609*, 17–26.
47. Ashoka, N.B.; Swamy, B.E.K.; Jayadevappa, H. Nanorod TiO_2 Sensor for Dopamine: A Voltammetric Study. *New J. Chem.* **2017**, *41*, 11817–11827. [CrossRef]
48. Prinith, N.S.; Manjunatha, J.G.; Hareesha, N. Electrochemical validation of L-tyrosine with dopamine using composite surfactant modifed carbon nanotube electrode. *J. Iran. Chem. Soc.* **2021**, *18*, 3493–3503. [CrossRef]
49. Khudaish, E.A.; Rather, J.A. Electrochemical studies of dopamine under stagnant and convective conditions at a sensor based on gold nanoparticles hosted in poly(triaminopyrimidine). *J. Electroanal. Chem.* **2016**, *776*, 206–212. [CrossRef]
50. Ashoka, N.B.; Swamy, B.E.K.; Jayadevappa, H. Tungsten oxide (WO_3) Modified Carbon Paste Electrode for Electrochemical Investigation of Dopamine in Presence of Uric Acid and Folic Acid. *Anal. Bioanal. Electrochem.* **2017**, *9*, 1057–1069.

51. Gururaj, K.J.; Swamy, B.E.K.; Shashanka, R.; Sharma, S.C.; Flores-Moreno, R. Dual descriptor analysis of cetylpyridinium modified carbon paste electrodes for ascorbic acid sensing applications. *J. Mol. Liq.* **2021**, *334*, 116348.
52. Shashanka, R.; Gururaj, K.J.; Prakashaiah, B.G.; Kumar, M.; Swamy, B.E.K. Electrocatalytic determination of ascorbic acid using a green synthesised magnetite nano-flake modified carbon paste electrode by cyclic voltammetric method. *Mater. Res. Innov.* **2021**, *26*, 229–239. [CrossRef]
53. Gururaj, K.J.; Swamy, B.E.K.; Chandrashekar, B.N.; Roberto, F.-M. Theoretical and cyclic voltammetric studies on electrocatalysis of benzethonium chloride at carbon paste electrode for detection of dopamine in presence of ascorbic acid. *J. Mol. Liq.* **2017**, *240*, 395–401.